PROCEEDINGS OF SPIE

SPIEDigitalLibrary.org/conference-proceedings-of-spie

RAR nano-textured diamond pulsed LIDT

Anthony Manni, Bruce MacLeod, Douglas Hobbs

Anthony D. Manni, Bruce D. MacLeod, Douglas S. Hobbs, "RAR nano-textured diamond pulsed LIDT," Proc. SPIE 12300, Laser-Induced Damage in Optical Materials 2022, 1230008 (2 December 2022); doi: 10.1117/12.2641596

SPIE.

Event: SPIE Laser Damage, 2022, Rochester, New York, United States

RAR Nano-Textured Diamond Pulsed LiDT Measurements

Anthony D. Manni*, Bruce D. MacLeod, and Douglas S. Hobbs
TelAztec LLC, 15 A Street, Burlington, MA, USA 01803-3404

ABSTRACT

Subwavelength, low-haze, anti-reflective (AR) nano-textured surfaces are an effective replacement for thin-film AR coatings (TFARCs) with the potential to increase reliability and minimize thermo-optic effects in kW-class diamond-based laser systems. Etched directly into optical surfaces, AR nano-textured surfaces can yield high optical damage resistance combined with high transmission, low back reflection, and low absorption values equivalent to the bulk substrate material. In this initial study, Random AR (RAR) nano-structures were etched into monocrystalline chemical vapor deposited (CVD) diamond windows. Photothermal common-path interferometry (PCI) measurements at 1064nm were conducted in order to characterize the level of absorption at the surfaces and through the bulk of diamond substrates. Nano-second pulsed laser induced damage threshold (LiDT) measurements at 1064nm were conducted, and damage sites were analyzed via scanning electron microscopy (SEM) to understand damage mechanisms in both as-polished and RAR nano-textured diamond samples.

Keywords: RAR Nano-Texture, Antireflection, Diamond Optics, Nano-Technology, Metasurfaces, Laser Damage, Motheye, AR

1.0 INTRODUCTION

Commercial availability of high quality, single-crystalline diamond fabricated by chemical vapor deposition has enabled novel applications in academic and industrial fields ranging from high power lasers to quantum optical communications and sensing [1-5]. Additionally, polycrystalline CVD diamond has long been the material of choice for high power CO_2 lasers operating at long-wave infrared (LWIR) wavelengths in the 10μm range. Diamond possesses a variety of material properties desirable for high power lasers such as high thermal conductivity of 2000 W/m•K relatively wide band gap of 5.45eV, extremely broad transparency window of 100nm to >100μm, low thermo-optic coefficient dn/dT ~ 8e-6 K^{-1}, and large Raman gain on the order of 13cm/GW [6]. However, its high Fresnel loss of ~16% per surface renders it difficult to use in high power laser systems where back-reflections can cause catastrophic damage to upstream optics. Therefore, it is critical to reduce the reflectivity of diamond surfaces while preserving the desired bulk material properties. Anti-reflective nano-textured surfaces are proposed as the optimal solution to this issue, as they do not require the deposition of any dissimilar material, which is the case with AR coatings. Integrating nano-structures directly into the surface of a material can reduce Fresnel losses over extremely wide optical and angular bands, while preserving inherent bulk material properties [7-10].

For pulsed lasers, damage is often associated with photoionization and dielectric breakdown at interfaces from high electric fields in the laser beam. On coated optics, this surface effect is enhanced by absorption in the functional coatings, and by defects in both the coating and polished surface of the optic. The LIDT of coatings for pulsed applications is well researched, and is typically quoted when purchasing an optic or specifying a thin film coating deposition. A growing body of data has shown that the pulsed LiDT of fused silica optics can be increased up to 5 times by replacing AR coatings with RAR nano-textures consisting of a random distribution of nanometer-scale features etched uniformly into the optic surfaces [11-15]. For longer pulses and CW laser operation, the LiDT of optics is typically dominated by thermal effects related to absorption in the surface coatings that leads to material ablation, melting, or thermally induced stress fractures in the bulk. RAR nano-textured optics typically eliminate surface absorption and should therefore survive much higher continuous-wave (CW) laser power compared to pulsed.

The graded index optical function introduced by RAR nano-texturing enables unrivaled optical performance compared to thin-film AR coatings that rely on interference effects [7]. Average single-surface reflection losses below 0.1% over the UV through NIR spectral range from 0.2 to 0.9μm, or the visible-NIR range of 0.4-1.6μm are routinely obtained, with losses as low as 0.001% (-50dB) at specified wavelengths. Off-axis performance is also superior for graded index textured surfaces, with fractions of a percent reflection change seen from +/-30°, ~1% change from +/-60°, and without the color shift that is characteristic of thin-films.

* admanni@telaztec.com; phone 1-781-229-9905; www.telaztec.com

Laser-Induced Damage in Optical Materials 2022, edited by Christopher Wren Carr, Detlev Ristau, Carmen S. Menoni, Proc. of SPIE Vol. 12300, 1230008
 · 0277-786X · doi: 10.1117/12.2641596

2.0 NUMERICAL MODELING OF RAR NANO-TEXTURED OPTICS

Anti-reflective metasurfaces such as the RAR nano-texture incorporate arrays of cone-like features which transition an optical wave from air to glass. The closely-packed features are much smaller than the wavelength of incident light, causing the wave to act as if it is traveling through a continuous material with a graded effective refractive index. Therefore, the RAR nano-texture can be approximated by effective medium theories such as the Maxwell-Garnett formalism [16]. For a more detailed understanding of the relationship between texture geometry and optical performance, however, more rigorous numerical methods are required.

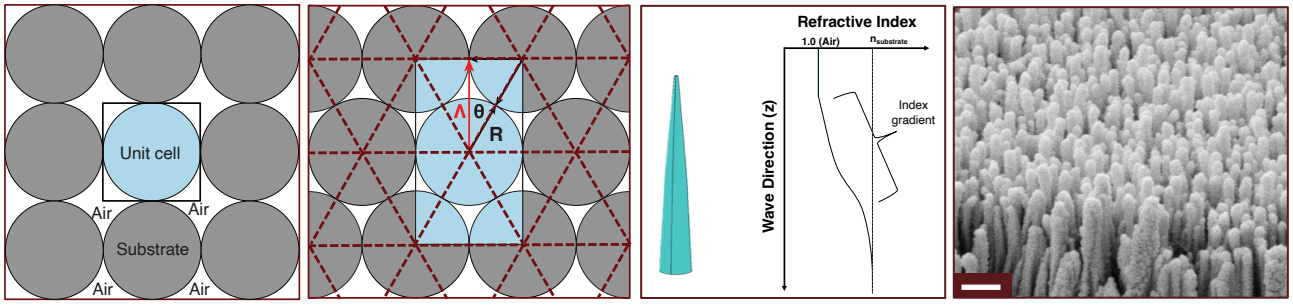

Figure 1. *Examples of (a) square-grid and (b) hexagonal lattice patterns and unit cells. (c) Example of an RAR nano-cone with varying slope, and the corresponding graded effective refractive index. (d) Scanning electron micrographs of the RAR nano-texture etched into diamond, scale bar = 200nm.*

Translationally symmetric, periodic metasurfaces are simulated by solving Maxwell's equations within a small area or volume called a unit cell, which is achieved by applying Floquet or Bloch periodic boundary conditions (PBCs) to the cell's outer boundaries in principal directions coplanar with the surface, in order to approximate the behavior of an infinite tiling of the unit cell. Typically, a square-grid lattice is defined for the sake of simplification, an example of which is depicted in Figure 1a. However, when modeling densely-packed nano-structures, such as the RAR nano-texture in the SEM in Figure 1d, a more accurate lattice is the triangular point or "honeycomb" pattern, i.e. a hexagonally-symmetric lattice achieving the highest packing density of equally-sized circular objects, as shown in Figure 1b. Honeycomb lattice unit cells can be hexagonal with three sets of PBCs, or rectangular with two sets of PBCs, for example.

By varying the feature radius as a function of height in 3-dimensions, an effective index gradient is formed in the direction of wave propagation, e.g. the z-axis, as depicted in Figure 1c. In Fourier-space methods such as rigorous coupled wave analysis (RCWA), the index gradient achieved by dividing the structure along the z-axis into several discrete layers, and the material distribution of each layer is constant in the z-direction. Maxwell's equations are then solved semi-analytically by Fourier transforming the transverse periodic structure and formulating an eigenvalue matrix equation for each layer, followed by calculating eigenmode coefficients which couple one layer to the next in a larger transfer matrix equation.

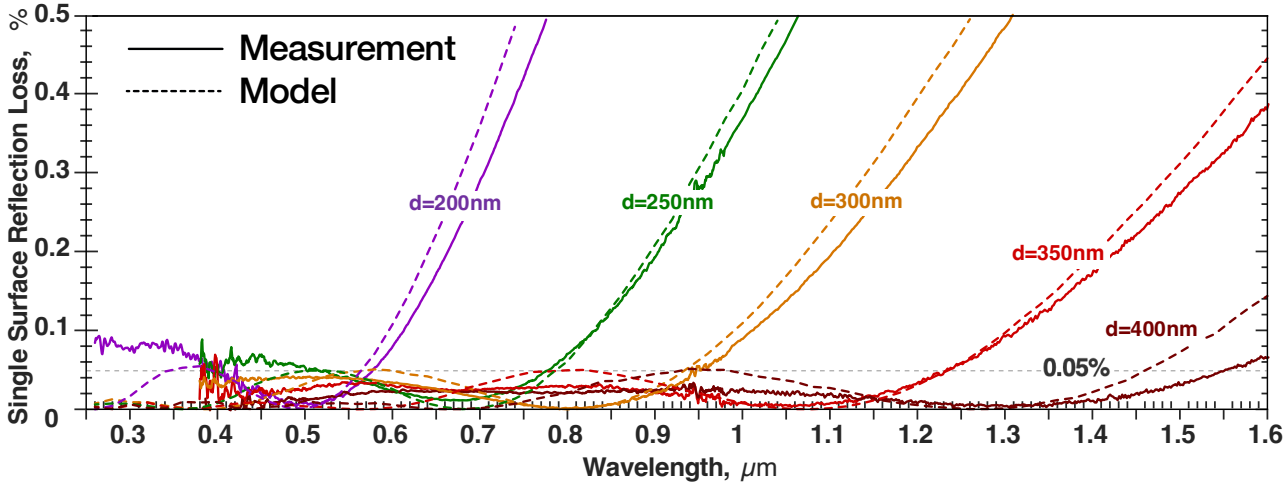

Figure 2. *Single-surface spectral reflectance of RAR nano-texture with varying texture depth, d.*

In finite element method (FEM) software such as COMSOL Multiphysics® [17], the 2D or 3D unit cell geometry is divided into a finite element mesh, rather than layers, and the electromagnetic field values are calculated at each mesh point by formulating a large matrix wave equation using variational methods and solving with advanced linear algebraic algorithms. Measurable properties such as reflectance and transmittance are then calculated by post-processing the simulated field data. Figure 2 shows the predicted and measured single-surface reflectance for a variety of RAR nano-texture depths in fused silica, the most well-established material for RAR nano-texturing. Note the strong agreement between theoretical and measured performance within 0.1%, highlighting the accuracy of the 3D FEM.

An additional feature of any graded index texture is its ability to function over a broad range of incident angles, due to the fact that the nanostructures do not rely on interference to achieve high transmission. Figure 3 displays reflectance spectra of an approximately 250nm-deep nano-texture etched in fused silica, evaluated at various angles of incidence by a third party (Optimax). Modeled and measured data are shown by dotted and solid lines, respectively. The overall trends in theory and production match well, showing an average increase in reflectance of merely 0.1% out to incident angles of 30°, and a monotonic increase in reflectance across the spectrum at angles ≥30°. Such angular response makes the RAR texture an optimal choice for curved surfaces and applications which incorporate transmissive optics positioned at steep angles with respect to incident light.

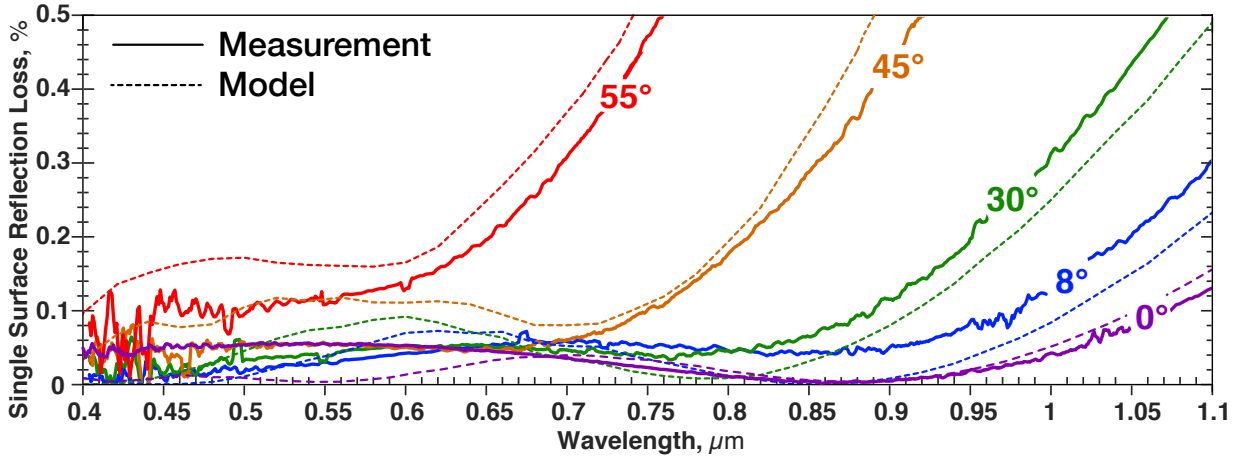

Figure 3. *Single-surface UV-visible spectral reflectance of 250nm-deep nano-texture at various angles of incidence, reflectance values are in absolute percentage with a y-axis maximum of 1%.*

3.0 RAR NANO-TEXTURED DIAMOND TRANSMISSION MEASUREMENTS

Optical grade, single-crystalline CVD diamond substrates were acquired in the form of (100)-oriented 3x3mm^2 by 1mm-thick plane-parallel windows, polished to a surface roughness of < 2nm Ra, wedge below 5 arcmin, and planarity < 0.25 λ @ 632.8nm (Diamond Materials GmbH, Freiburg, Germany). Each sample was measured in transmission from the UV to the LWIR by 2 separate fiber-input grating-based spectrometers covering the VIS-NIR (400-950nm, Filmetrics), and NIR (950-1650nm, Ocean Optics) wavelength regions, and an open-beam Thermo-Nicolet Fourier Transform IR (FTIR) spectrometer covering wavelengths from 1.65 to 25μm. An example of a measured total transmission trace of the as-received material is shown below in Figure 4 by the dashed-dotted black trace around 70%. The samples were then cleaned in a 3:1 piranha solution of 90% sulfuric acid and 30% hydrogen peroxide for 60 seconds to remove organic surface contaminants, followed by distilled water and methanol rinse. They were then submerged in 30% ammonia hydroxide for 60 seconds, rinsed with methanol, isopropanol, and blown dry with filtered N_2. Several samples were then subjected to a proprietary plasma-based RAR nano-texturing process specifically developed for diamond, on one surface only.

Each sample was placed directly on the 12”-diameter base electrode of an inductively coupled plasma reactive ion etch (ICP-RIE) tool. The first etched sample was exposed to a plasma recipe labeled “RARD1” for a duration of ten minutes, on one surface only, with the intent of etching roughly 500nm-deep to achieve maximum transmission in the 1-1.3μm range for Raman laser applications. The measured transmission in the visible-NIR is shown by the dashed green line in Figure 4, which has a peak transmission value of roughly 83% at 1550nm. The diminished transmission efficiency at shorter wavelengths is due to Rayleigh scattering at the surface, implying the texture features were too large and far apart. Note the maximum theoretical total transmission for perfect one-surface anti-reflection with a polished second surface, represented by the dotted gold line.

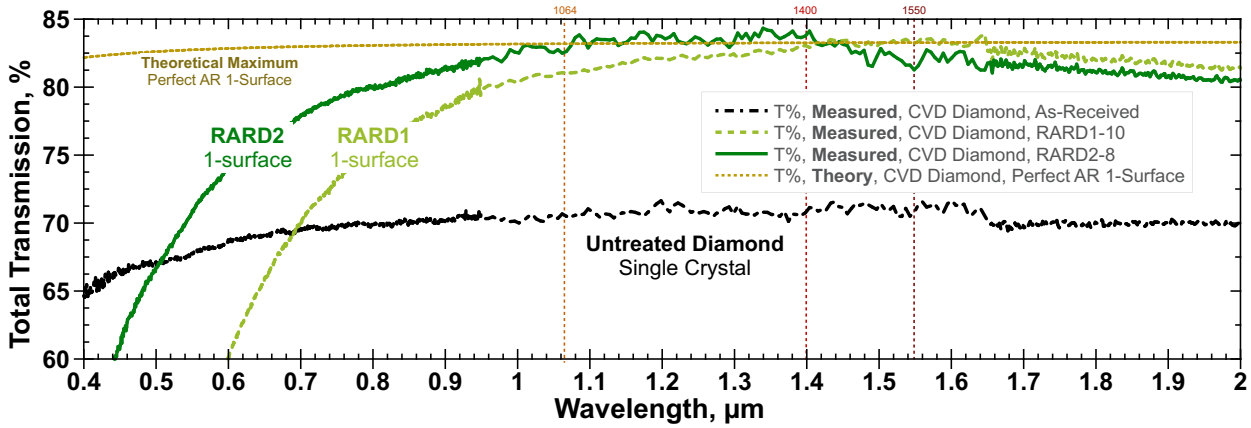

Figure 4. *VIS-NIR measured total transmission of single-surface RAR nano-textured CVD diamond windows.*

The refractive index used to calculate maximum theoretical transmission was modeled by a single-term Sellmeier equation empirically derived by Turri, Bass et. al. for the wavelength range 350-1650nm [18]. Subsequently, in order to reduce scatter losses, the plasma parameters were adjusted to increase ion density and lower the reactive ion bombardment energy. A new sample was then exposed to this second "RARD2" process for a duration of 8 minutes, and its measured total transmission is shown by the solid green curve in Figure 4. Note that the maximum transmission bandwidth increased from roughly 100nm in the RARD1 process to greater than 300nm in the RARD2 process, and the scatter edge decreased in wavelength by about 150nm. Further improvements to the plasma etch recipe are likely to continue this trend, extending the bandwidth further and driving down scatter loss.

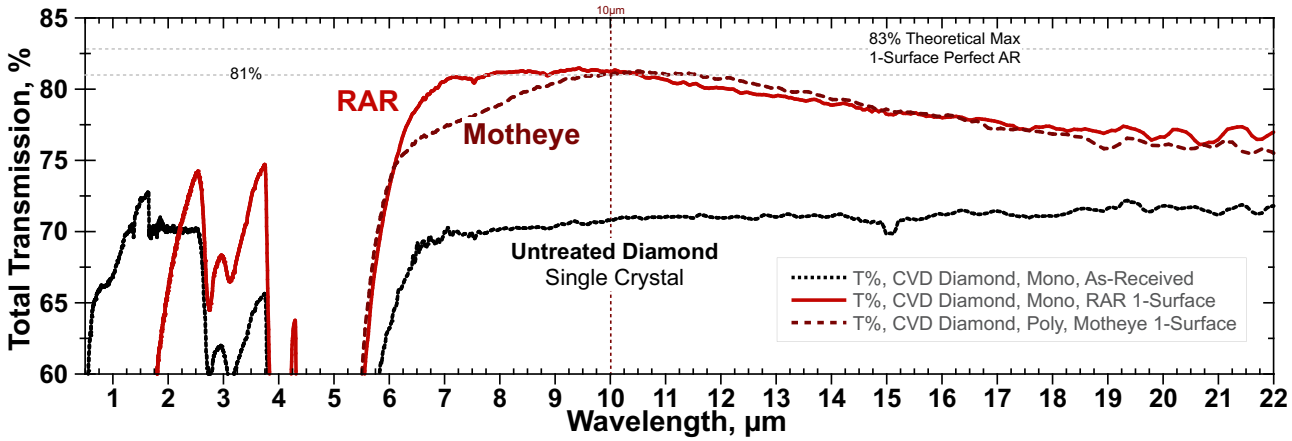

Figure 5. *Infrared total transmission spectra of single-surface RAR nano-textured optical-grade CVD diamond windows, in comparison with periodic Motheye structured poly-crystalline diamond.*

In addition to targeting applications in the NIR, AR performance in the LWIR for high power CO_2 laser applications was achieved by extending the plasma etch process to establish an RAR nano-texture that was greater than a micron deep. One surface of a single crystal CVD sample was exposed to the same RARD2 etch as before, but the total etch duration was increased to 70 minutes. The sample was removed after 20 and 50 minutes to ensure that the texture was not being erased during the prolonged exposure. Plasma etch residue was then removed by boiling the sample in piranha solution followed by water and solvent rinsing. Measured total transmission for this sample is shown by the solid red curve in Figure 5 above, displaying a peak transmission of roughly 81.5%, which is 1.5% off the theoretical maximum transmission of 83%, ignoring bulk absorption. For comparison, the dashed maroon line plots the measured total transmission of a *poly*-crystalline diamond sample with a periodic motheye AR micro-texture applied to one surface. This texture required an initial patterning step involving interference lithography (IL), followed by metallization and plasma etching. Note the similarity in peak transmission level, though the bandwidth of the RAR textured sample is a bit wider than that of the motheye sample. The single-step RAR etch process greatly reduces fabrication costs and enables the scaled production of surface relief AR texturing of diamond CO_2 laser optics.

4.0 DIAMOND ABSORPTION MEASUREMENTS

Thermal effects related to bulk and surface absorption in thin film coatings are a known mechanism that results in laser beam degradation and ultimately damage to optical components. Through years of absorption testing as a process validation, graded index nano-textured surfaces in various materials have been shown to exhibit an absence of elevated surface absorption over the bulk level [19-20]. The zero-added absorption property results directly in improved beam quality, extended lifetime, and increased power scaling, and is the driving force behind the DoD and commercial laser industries' acceptance of nano-textured optics for many applications. Measuring the surface and bulk absorption of highly transparent materials is most commonly achieved by means of Photothermal Common-path Interferometry (PCI) [21]. In this work, the services of Island Interferometry in Hilo, HI were employed to attempt characterizing the bulk and surface absorption of thin CVD diamond substrates. PCI uses a high power 1064nm pump beam focused onto an optic to produce a localized heating effect due to absorption of photons. A low power probe beam intersects the pump beam at the pump's focal plane, as shown on the left side of Figure 5, and creates an interference pattern in the probe beam due to the localized thermally induced index change. The absorption level is then calculated from the spacing of the interference fringes. The overlap spot of the beams is the test location, and the sample is scanned either longitudinally from front to back through the beam, or transversely across a surface.

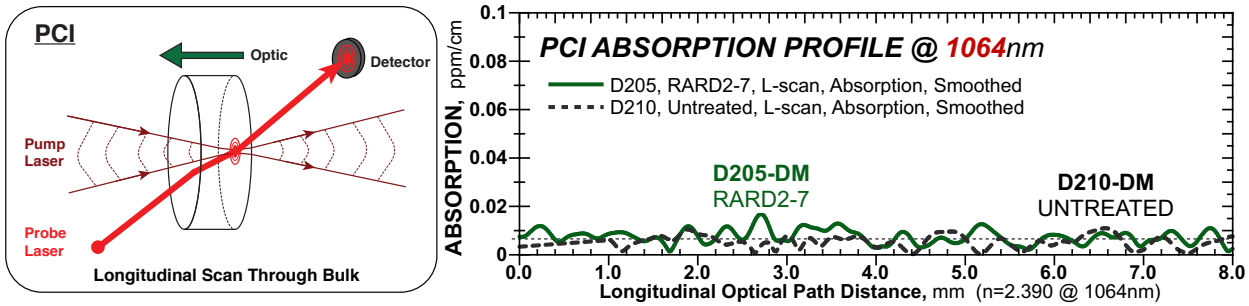

Figure 6: *Longitudinal PCI absorption scan schematic (left), and measured PCI scans through untreated and RAR nano-textured single crystal CVD diamond samples.*

Longitudinal PCI scans of untreated and RAR nano-textured CVD diamond samples are shown above in Figure 6. Note that due to the high thermal conductivity of diamond, it was not possible to establish a thermal lens for a long enough period of time to observe the interference pattern and accurately calculate absorption values. Therefore, the results are inconclusive and may require alternative absorption measurement techniques such as laser calorimetry (LC). The absorption coefficient of single crystal CVD diamond has been reported elsewhere and ranges from 0.001 cm^{-1} to as much as .08 cm^{-1}, depending most strongly on extrinsic absorption by nitrogen in solid solution [5].

5.0 DIAMOND PULSED LASER DAMAGE TESTING

A set of five, 3x3mm^2 x 1mm thick, monocrystalline CVD diamond windows were submitted to the Lumibird Group in Bozeman, Montana for their commercial 's-on-1' type pulsed laser induced damage threshold measurements. "Damage" is defined as any permanent surface change that can be observed at high magnification (150x), and "threshold" is used to describe the lowest fluence required to induce damage at any site. Lumibird's testing adheres to the ISO 21254 standard and involves irradiating a test sample at several different fluence levels, with multiple sites per level. In order to increase the number of damage frequency values above the zero damage threshold and below 100% damage probability, the fluence increments and number of exposure sites per fluence level are adjusted accordingly, thereby obtaining better linear fits for the reported LiDT. As shown on the left side of Figure 7, damage probability is plotted as a function of fluence, and a least squares linear fit is applied, and the fluence-axis intercept of the fit is defined as the damage threshold fluence. Laser damage testing in this work consisted of a Nd:YAG laser operating at 1064nm wavelength, 18.4 ns pulse width (FWHM), 20 Hz pulse repetition rate, 260µm focused spot diameter ($1/e^2$), TEM00 spatial mode, linear polarization, 0 degree AOI, ~50 exposure sites on a grid with spacing >2x spot diameter, 200 shots per site, and 4-6 fluence levels per sample. The LiDT sample matrix included two windows as-received, and three RAR nano-textured windows. The 1064nm pulsed laser damage thresholds are shown in the histogram on the right in Figure 7, after having been scaled to their equivalent values for an effective pulse-width of 5ns, for comparison with literature values. The common $\sqrt{t}$ method for scaling the damage threshold was used, with t being the pulse width. The two untreated samples survived to an average fluence of 14.8 Joules (J)/cm^2, while the three RAR nano-texture samples showed an average damage threshold of only 2.2 J/cm^2.

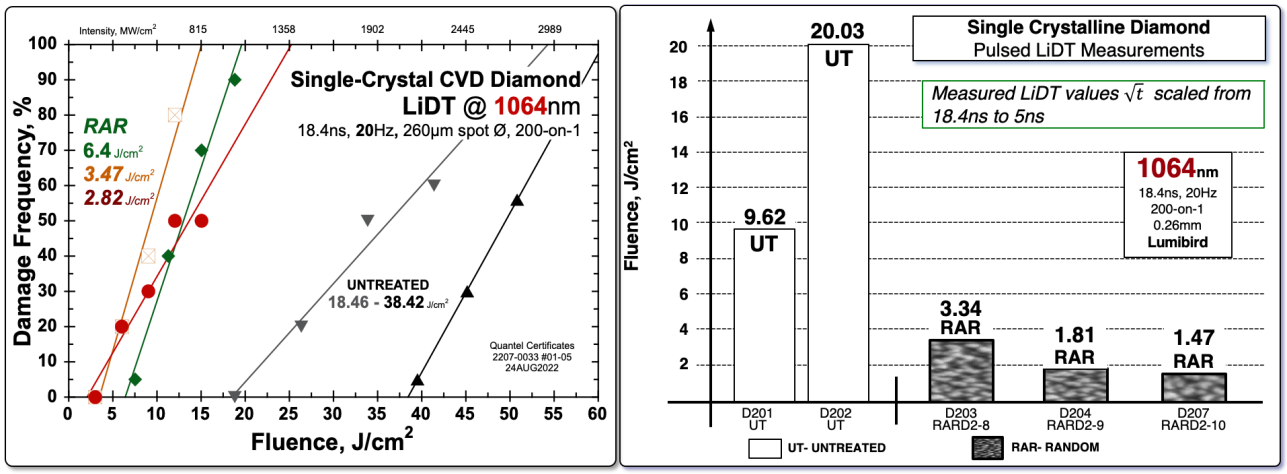

Figure 7: *1064nm pulsed laser damage test results on untreated and RAR textured single-crystal CVD diamond.*

The 20 J/cm^2, 5 ns LiDT value at 200 shots per site is similar to single-shot values reported in the literature by A.J. Kemp, et. al. of 26 J/cm^2 at 6.5 ns [22]. The discrepancy between LiDT for the two untreated samples is difficult to describe with such a small sample size, but they are both at least 3 times higher than the LiDT values of all the RAR nano-textured samples. Note that the textured samples D203, D204, and D207 were plasma etched for 8, 9 and 10 minutes, respectively. A clear trend between LiDT and plasma exposure is observed, which may be the result of the formation of an absorptive graphitic layer on top of the texture due to ion bombardment during the etch process. Graphitization of diamond surfaces due to ion bombardment is a well-documented concept [23], but was not discovered by the authors before conducting LiDT tests, and therefore steps were not taken to try to prove the existence or mitigate the effects of such a layer. Subsequent work will require detailed analysis of chemical states on the surface of RAR nano-textured samples before and after degraphitization.

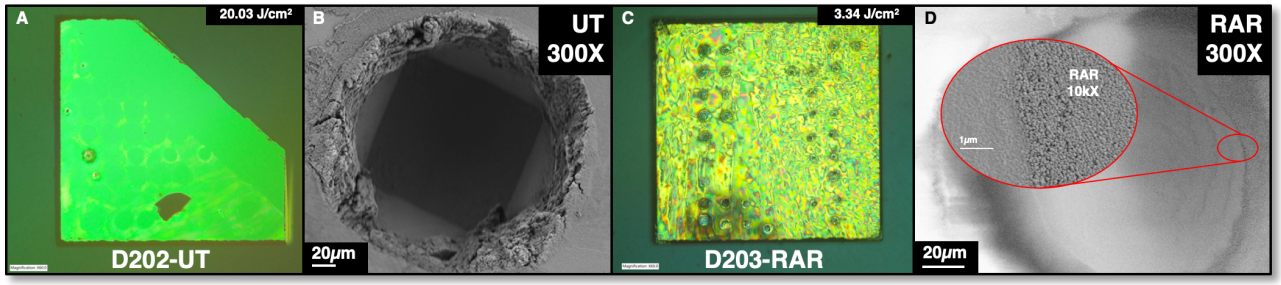

Figure 8: *Polarized optical micrographs of LiDT-tested (a) untreated and (c) RAR nano-textured CVD diamond samples. Scanning electron micrographs (b), (d), of damage sites in corresponding samples. Inset in (d) shows damaged nano-texture at 10kX mag.*

Optical and electron micrographs are presented above in Figure 8. The untreated diamond samples experienced catastrophic damage in the form of micro-explosion and fracturing along crystal planes at high fluence, as shown by the polarization optical micrograph in Figure 8a, taken at Lumibird. A SEM of one of the lower-fluence damage sites on the same sample is shown in Figure 8b, indicating that damage may have been initiated by self-focusing and plasma formation immediately below the surface. Note the smooth, square bottom of the damage crater which is smaller than the incident laser spot, while the top of the crater is almost exactly 260µm in diameter. In contrast, the RAR nano-textured samples did not damage catastrophically. Optical and electron micrographs of a damaged RAR sample are shown in Figure 8c and 8d, respectively. The high-mag SEM (10kX) of the damaged RAR nano-texture in the inset of Fig. 8d shows that a top layer of the texture merely melted and filled in the voids between surface features under low fluence, increasing the reflectivity and thus satisfying the damage criteria. This implies there was significantly higher surface absorption in the plasma-induced graphitic layer, which was not measurable by PCI because of diamond's high thermal conductivity, as described in the previous section. Future efforts will explore techniques for removal of the graphitic layer, as well as any resulting effects on LiDT.

6.0 SUMMARY

Random anti-reflective nano-textures were integrated into CVD diamond surfaces by a scalable, lithography-free plasma etching process to achieve broadband high transmission in the NIR and LWIR. In this initial study, the optical performance and laser durability of monocrystalline CVD diamond samples were evaluated by means of PCI and nanosecond pulsed LiDT testing. PCI measurements at 1064nm were inconclusive due to the extreme thermal conductivity of bulk diamond, while LiDT tests showed a clear reduction in laser durability with prolonged plasma exposure, likely due to the presence of a graphitic layer caused by ion bombardment. The 200-on-1 LiDTs of two polished CVD diamond samples were found at an average of 28.4 J/cm^2 for 18.4ns pulses, and the RAR nano-textured samples averaged to 4.23 J/cm^2 under the same irradiation conditions. This work provides a foundation on which to improve the power-scaling properties of RAR nano-textured diamond optics for high energy pulsed and CW laser applications.

7.0 ACKNOWLEDGEMENTS

The authors gratefully acknowledge Gary Shaffer of Lumibird, for his detailed and careful pulsed laser damage testing and polarization imaging. Detailed PCI absorption scans and data analysis was provided through the services of Chris Franz and Alexei Alexandrovski at Stanford Photothermal Solutions (SPTS). Dr. Richardson's lab at UCF CREOL contributed high quality CVD diamond substrates and insightful technical discussions related to Raman lasers. The authors also thank Eckhard Wörner from Diamond Materials for providing single-crystal samples used in this work.

8.0 REFERENCES

[1] Scarsbrook, G.A., et. al., "Development of high quality single crystal diamond for novel laser applications," Proc. SPIE **7838**, (2010)
[2] Lu, Z., et. al., "Diamond Raman laser: A promising high-beam-quality and low-thermal-effect laser". High Power Laser Science and Engineering, 9, **E35**. (2021)
[3] Lukin, M.D., Sørensen, A.S., et. al., "One-Way Quantum Repeater Based on Near-Deterministic Photon-Emitter Interfaces." Phys. Rev. X 10, **021071** (2020)
[4] Taylor, J., Cappellaro, P., Childress, L. et al., "High-sensitivity diamond magnetometer with nanoscale resolution." Nature Phys 4, 810–816 (2008)
[5] de Wit, H., et. al., "Single crystal and polycrystalline CVD diamond for demanding optical applications," Proc. SPIE 8016, **80160L** (2011)
[6] Element Six. "Element Six Diamond Handbook." Berkshire, UK; (2021)
[7] Clapham, P., Hutley, M., "Reduction of lens reflexion by the Moth Eye principle, " Nature **244**, 28 (1973)
[8] Hobbs, D. S., MacLeod, B. D., "Design, Fabrication, and Measured Performance of Anti-Reflecting Surface Textures in Infrared Transmitting Materials, " Proc. SPIE **5786**, 349 (2005)
[9] Hobbs, D. S., MacLeod, B. D., "Update on the Development of High Performance Anti-Reflecting Surface Relief Micro-Structures, " Proc. SPIE **6545**, 65450Y (2007)
[10] MacLeod,B.D., Hobbs,D.S., "Long life, high performance anti-reflection…," Proc. SPIE **6940**, 69400Y (2008)
[11] Hobbs, D. S., MacLeod, B. D., "High laser damage…. micro-structures.., " Proc. SPIE, **6720**, 67200L (2007)
[12] Hobbs, D.S., "Laser damage threshold measurements of anti-reflection microstructures operating in the near UV and mid-infrared, " Proc. SPIE **7842**, 78421Z (2010)
[13] Hobbs, D.S., et.al., "Laser damage resistant anti-reflection microstructures in Raytheon ceramic YAG, sapphire, ALON, and quartz, " Proc. SPIE **8016**, 80160T (2011)
[14] Hobbs, D. S., MacLeod, B. D., Sabatino, E., "Continued advancement of laser damage resistant optically functional microstructures, " Proc. SPIE **8530**, 85300O (2012)
[15] Hobbs, D.S., et. al., "Pulsed... nanostructured… reflectors… 355nm.., " Proc. SPIE, **10447**, 104470W (2017)
[16] Sihvola, A. H.. "Electromagnetic Mixing Formulas and Applications." United Kingdom, Institution of Electrical Engineers, (1999)
[17] COMSOL Multiphysics® v. 5.4. www.comsol.com. COMSOL AB, Stockholm, Sweden.
[18] Bass, M., Turri, G., et. al., "Index of refraction … single crystal microwave-assisted CVD diamond," Opt. Mater. Express 7, **855-859** (2017)
[19] Hobbs, D. S., et.al., "Contamination resistant antireflection nano-textures.., " Proc. SPIE, **8885**, 88850J (2013)
[20] MacLeod, B.D., et. al., "CW laser damage... RAR nano-textured... YAG" Proc. SPIE, **10447**, 1044705 (2017)
[21] Alexandrovski, A., et. al., "Photothermal common-path interferometry….." Proc. SPIE **7193**, 71930D (2009)
[22] Kemp, A.J., et. al., "Laser Induced Damage Threshold of CVD-Grown Single Crystal Diamond Surfaces …," in Advanced Solid State Lasers, Optica, paper ATu2A.6 (2015)
[23] Lee, S.T., Bello, I., et. al., "Effects at reactive ion etching of CVD diamond," Thin Solid Films, Volume 368, Issue 2, Pages 222-226, (2000)